JOURNAL OF THE CANADIAN SOCIETY OF EXPLORATION GEOPHYSICISTS
VOL. 22, NO. 1 (DEC. 1986) P. 44-55

# INVERSE VELOCITY STACKING FOR MULTIPLE ELIMINATION

DAN HAMPSON[1]

## ABSTRACT

Inverse Velocity Stacking is a technique proposed by Thorson (1984) for modelling events with hyperbolic move-out on seismic profiles. In this procedure, the input profile is represented as a linear combination of hyperbolic events with constant amplitude. The weighting coefficients are calculated to produce a model that approximates the input profile in the least-squares sense.

In this paper, the use of this approach is demonstrated for modelling and attenuating long-period multiples. To reduce the computational effort, the algorithm is modified to incorporate a parabolic rather than a hyperbolic modelling scheme. This allows an explicit solution to be derived which results in a significant computational improvement over the original iterative procedure. The parabolic modelling may be justified if the input profile is NMO-corrected.

The algorithm is demonstrated on both synthetic and real data, where it is shown to be very effective in attenuating multiples with residual move-out in excess of 30 ms from zero-offset to far-offset. For shorter-period multiples with less residual move-out, the possibility of distinguishing multiple and primary energy is reduced, especially for noisy data. An attractive feature of the algorithm is that its performance is uniform over the entire offset range. As a result, the algorithm appears to be a significant improvement over existing F-K procedures.

## INTRODUCTION

Inverse Velocity Stacking is the name applied to a procedure devised by Thorson (1984), and described in Thorson and Claerbout (1985), for modelling hyperbolic events on seismic records. In this algorithm, the recorded seismic profile is modelled as a linear combination of simple hyperbolic events of constant amplitude. A set of weighting coefficients is derived such that the resulting model approximates the input profile in the least-squares sense. Each hyperbolic event is characterized by two parameters: the zero-offset time of the event, $T_0$, and the slowness,

$$p = 1/V \qquad (1)$$

where V is the RMS velocity associated with that event. As discussed by Thorson (1984), the set of weighting coefficients can be interpreted directly to give the energy associated with the various velocities at different zero-offset times. In this sense, the coefficients form an 'idealized' constant velocity stack, useful for velocity analysis. The derived model may be further used for noise reduction and interpolation of missing data.

An application that was not discussed by Thorson is that of long-period multiple elimination. This application depends on the fact that primary and long-period multiple events at a given zero-offset time will generally have different RMS velocities and will map to different regions of the domain spanned by the set of weighting coefficients. Inverse transforming after zeroing selected sets of coefficients will then isolate primary and multiple energy, as is commonly done with F-K filtering (Ryu, 1980). This procedure was used with some success by Hampson and Dunham (1985), but the computational effort made the approach impractical for volume processing.

A large part of the computational effort can in fact be traced to the hyperbolic form of the move-out equation. Modifying this equation to incorporate a parabolic rather than a hyperbolic form results in a significant simplification of the linear system, which must be solved, and a corresponding reduction in computational effort. In the remainder of this paper, I derive the modified linear system, justify its use on NMO-corrected data, and demonstrate its application to the problem of long-period multiple elimination.

## THEORY

The basic modelling equation proposed by Thorson is

$$d(h,t) = \iint dp\,d\tau\, U(p,\tau)\,\delta\left|\tau - \sqrt{t^2 - p^2h^2}\right| + n(h,t) \qquad (2)$$

where d (h,t) = measured seismogram at offset h and two-way time t

U (p,$\tau$) = hyperbolic transform coefficient at slowness p and zero-offset time $\tau$

n (h,t) = measurement noise at offset h and two-way time t

[1]Veritas Software Ltd., 615 - 3rd Avenue S.W., Calgary, Alberta

There are two ways of interpreting this equation. One way is to view it as a modelling system. Our seismic data are d(h,t), which could be a shot profile or a common-depth-point gather. In equation (2) we are attempting to model these data as a linear combination of functions of the form

$$\delta [\tau - \sqrt{t^2 - p^2h^2}] \tag{3}$$

The real numbers $U(p,\tau)$ are the weights associated with each of the functions. These functions in fact represent hyperbolae, as can be seen by imagining a situation in which all the weights are zero except for that associated with $p = p_o$ and $\tau = \tau_o$ :

$$U(p,\tau) = A\,\delta\,(p-p_o)\,\delta\,(\tau - \tau_o) \tag{4}$$

Inserting this into equation (2), and ignoring the noise component momentarily,we get

$$d(h,t) = A\,\delta\,[\tau_o - \sqrt{t^2 - p_o^2h^2}] \tag{5}$$

This represents a hyperbola with amplitude A and a trajectory defined by

$$t^2 = \tau_o^2 + p_o^2h^2 \tag{6}$$

In general, the double integral in equation (2) is a sum over all possible hyperbolae, each with its own weighting factor.

The presence of the noise term, n(h,t), indicates that we do not expect this modelling to be perfect; that is we do not expect the linear combination to yield precisely the input data. One reason for this is that the integrals will be performed over a limited range of slownesses, p, and times, $\tau$. The noise term represents the misfit between our 'best' model and the input data. As we shall see below, this 'best' model is derived by minimizing the energy in this noise term.

The second way to interpret equation (2) is to view it as a transform, analogous, for example, to the $\tau-p$ transform. In fact, the $\tau-p$ transform can be written as (Thorson, 1984):

$$d(h,t) = \int\int dp\,d\tau\,U(p,\tau)\,\delta\,[\tau - (t - p\,h)] + n(h,t) \tag{7}$$

Just as the $\tau-p$ transform can be calculated by summing along linear trajectories, the calculation of $U(p,\tau)$in equation (2) involves summing along hyperbolic trajectories. From this point of view, equation (2) is closely analogous to the $\tau-p$ transform. The presence of the noise term now implies that the transform space generated by the basis functions (3) is not a complete space. That is, if we transform a data set from the (h,t) domain to the hyperbolic $(p,\tau)$ domain and back, we do not retrieve the original data. The noise n(h,t) is the component of d(h,t) that is 'lost' in the transformation or, equivalently, the component of d(h,t) that is orthogonal to the space generated by the basis functions (3).

Regardless of which interpretation we use, the problem to be solved is: given the measured seismogram d(h,t), find the weights $U(p,\tau)$ that satisfy equation (2) while minimizing the misfit n(h,t). Thorson and Claerbout (1985) showed that this problem can be solved as an overdetermined linear system. Assuming that d(h,t) and $U(p,\tau)$ are defined at discrete values of h,t,p, and $\tau$, equation (2) can be reduced to the matrix equation:

$$d = L\,u + n \tag{8}$$

where d is a vector containing all values in the measured seismogram, u a vector containing all the weights, n the vector of noise values and L the matrix that incorporates the discrete form of the delta-function in (2). The standard least-squares solution to (8) is:

$$u = (L^TL)^{-1}\,L^Td \tag{9}$$

While the form of equation (9) suggests that this solution is straightforward, the dimensions of the matrices involved make an explicit solution impractical. L is a matrix of dimension:

$(N_T \times N_H)$ by $(N_T \times N_P)$

where $N_T$ = number of time samples in the input seismogram
$N_H$ = number of offsets in the input seismogram
$N_P$ = number of slownesses used in $U(p,\tau)$

In a typical 96-trace seismic shot of 3-second duration, L would be of the order of 150,000 by 150,000. Thorson and Claerbout (1985) suggested an iterative solution, which is still prohibitively time-consuming.

In order to reduce the computational load, I propose to replace the hyperbolic equation (2) by the parabolic form:

$$d(h,t) = \int\int dp\,d\tau\,U(p,\tau)\,\delta\,[\tau - (t - p\,h^2)] + n(h,t) \tag{10}$$

where p is no longer the slowness defined by equation (1), but simply a coefficient whose significance will become apparent later. Just as equation (2) modelled the input seismogram as a linear combination of hyperbolae, equation (10) models the seismogram as a linear combination of parabolae. The appropriateness of this function will be discussed below. The important feature to note here is that we can take the Fourier Transform of both sides of equation (10) and show that each Fourier com-

ponent can be calculated independently by solving a greatly reduced system. Let:

$$U(p,\tau) = \sum_{w} U(p,w)\, e^{iw\tau} \qquad (11)$$

and

$$d(h,t) = \sum_{w} d(h,w)\, e^{iwt} \qquad (12)$$

Inserting these equations into (10) and transforming the integral over p to a discrete sum gives the following result:

$$d(h,w) = \sum_{p} U(p,w)\, e^{-iwph^2} + n(h,w) \qquad (13)$$

Note that, in this equation, the unknown coefficients U(p,w) for a given frequency w depend only on the data components d(h,w) for that frequency. This 'decoupling' of the frequency components occurs because equation (10) is linear in both t and $\tau$. Equation (2), on the other hand, is not linear and no such decoupling would occur in the frequency domain.

Solving equation (13) is now straightforward. As before, we write the matrix equation:

$$d = Lu + n \qquad (14)$$

where d is the complex vector of all the components d(h,w) for a specific w, n the complex vector of noise components at frequency w, u the vector of components U(p,w), and L the matrix defined by:

$$L(j,k) = e^{-iwp_k h_j^2} \qquad (15)$$

Equation (14) is solved as a least-squares system:

$$(L^{\dagger}L)\, U = L^{\dagger}d \qquad (16)$$

taking account of the fact that we are now dealing with complex quantities. The dimension of the complex matrix, $L^{\dagger}L$, which must be inverted, is $N_p$ by $N_p$, where $N_p$ is the number of discrete values of P over which we perform the integration in (10). As discussed below, this is usually of the order of 20, so that inverting $L^{\dagger}L$ is equivalent to inverting a 40 by 40 real matrix, a task that is performed very efficiently in an array processor. For a given shot profile, system (16) must be set up and solved $N_w$ times, where $N_w$ is the number of discrete frequency values of interest.

## Application to Multiple Elimination

Thorson and Claerbout (1985) discussed a number of applications of the inverse velocity stack algorithm. In particular, Figure 1 illustrates the use of this algorithm for velocity analysis. On the left-hand panel a synthetic CDP gather is shown. The centre panel displays a conventional constant velocity stack (CVS) analysis, generated by NMO-correcting the CDP gather with a set of 20 constant velocities ranging from 6500 ft/s to 11,500 ft/s and stacking to form a single stacked trace for each velocity. As Thorson pointed out, one problem with the CVS tool is that events will not only image at their true velocity, but will show a significant spread of energy throughout all the neighbouring velocities as well. This does not cause a problem for interpreting isolated events like the one at 1.23 s, but the lateral smearing of closely spaced events with different velocities makes the interpretation difficult for complexes such as the group of events between 0.9 and 1.2 s. In the right hand panel we show a hypothetical plot of the coefficients $U(p,\tau)$, which would be calculated by using equation (2). As we can see, these form an 'ideal' CVS in that each event shows a maximum response at its own velocity and very little energy at neighbouring velocities. In fact, as Thorson pointed out, the conventional CVS is precisely the $L^{\dagger}d$ factor in equation (9). The coefficients $U(p,\tau)$ are calculated by multiplying this factor by $(L^{\dagger}L)^{-1}$ which effectively deconvolves the laterally smeared events and sharpens their image. In this form there is a separation of events at similar times according to their velocities, and separation of multiple from primary energy should be possible.

The mapping of seismic events into sharp isolated images in the $U(p,\tau)$ plot occurs because the events are hyperbolic and equation (2) models the data as a linear combination of hyperbolic shapes. This is analogous to the $\tau$ - p case in which linear events are mapped to discrete points. If the parabolic approximation of equation (10) were used on this data set, the events would be smeared and the separation might not be sufficient to distinguish multiple from primary energy. Accordingly, we propose to apply the parabolic form to NMO-corrected data. To see that the resulting events will be approximately parabolic, consider an event at zero-offset time T and RMS velocity V. If this event is corrected with velocity Vc, the event will now appear at time T(h), where,

$$T(h) = \sqrt{T^2 + h^2/V^2} - \sqrt{T^2 + h^2/Vc^2} \qquad (17)$$

$$= T\left\{1 + \sqrt{1 + h^2/V^2T^2} - \sqrt{1 + h^2/Vc^2T^2}\right\} \qquad (18)$$

Defining the residual velocity Vr by:

$$1/Vr^2 = 1/V^2 - 1/Vc^2 \qquad (19)$$

and expanding equation (18) in a Taylor series in (h/VrT), we get

$$T(h) = T + h^2/2TVr^2 + \ldots \qquad (20)$$

If $(h/VrT) \ll 1$, we are justified in dropping the higher-order terms. Thus, to the extent that equation (20) is

valid, we can expect the NMO-corrected events on the input seismogram to map to discrete points on the plot of $U(p,\tau)$ defined by equation (10). As events deviate from the ideal parabolic form, we can expect a smearing, with a resultant degradation in the ability to distinguish multiple from primary energy.

## Model Results

The application of equation (10) will now be demonstrated on the model data set shown on the left of Figure 2. This represents an NMO-corrected shot profile. Experience has shown that, when processing split-spread shot profiles, it is best to process each side of the spread separately. Accordingly, the synthetic in Figure 2 represents one side of a split-spread profile. Both primary and multiple energy can be seen in a strongly interfering pattern.

Figure 2 demonstrates the modelling interpretation of equation (10) — the input profile is represented as a weighted sum of simple parabolae of constant amplitude. One might at first wonder how a combination of con-

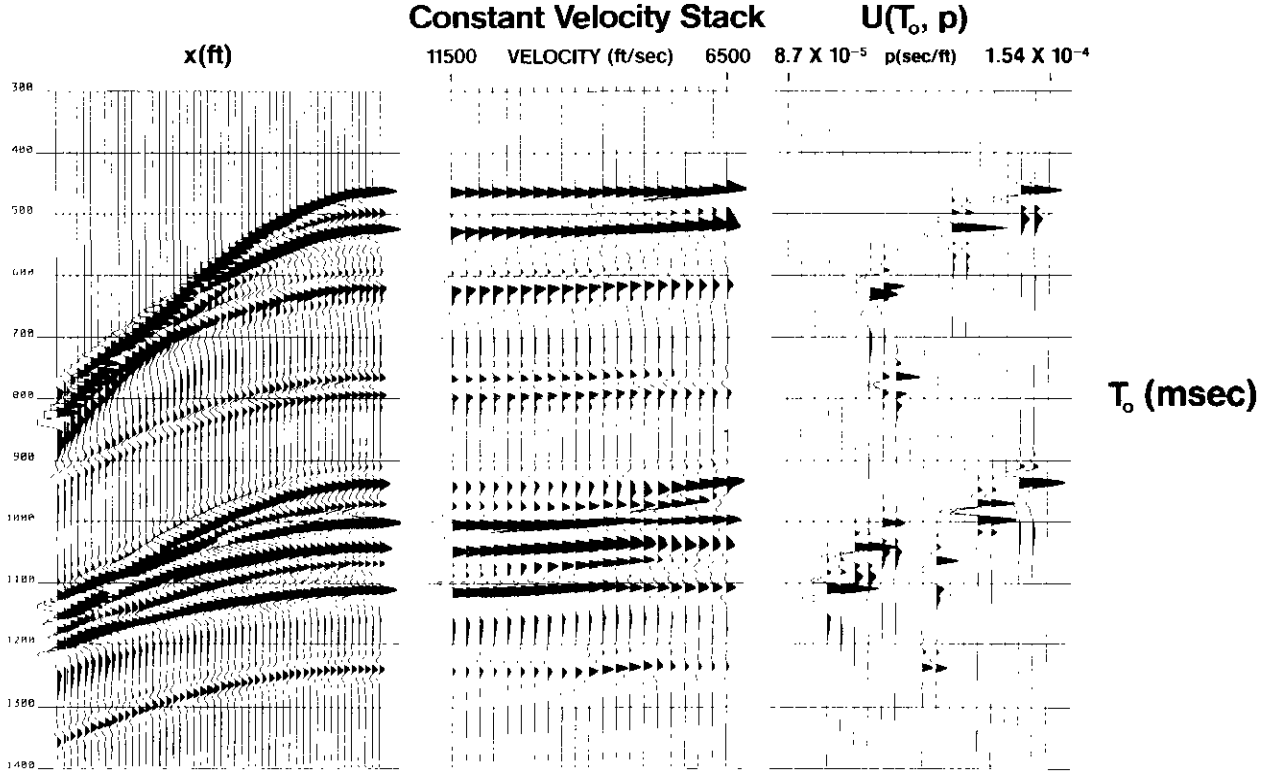


**Fig. 1.** Interpretation of the inverse velocity stack coefficients as an 'ideal' constant velocity stack.

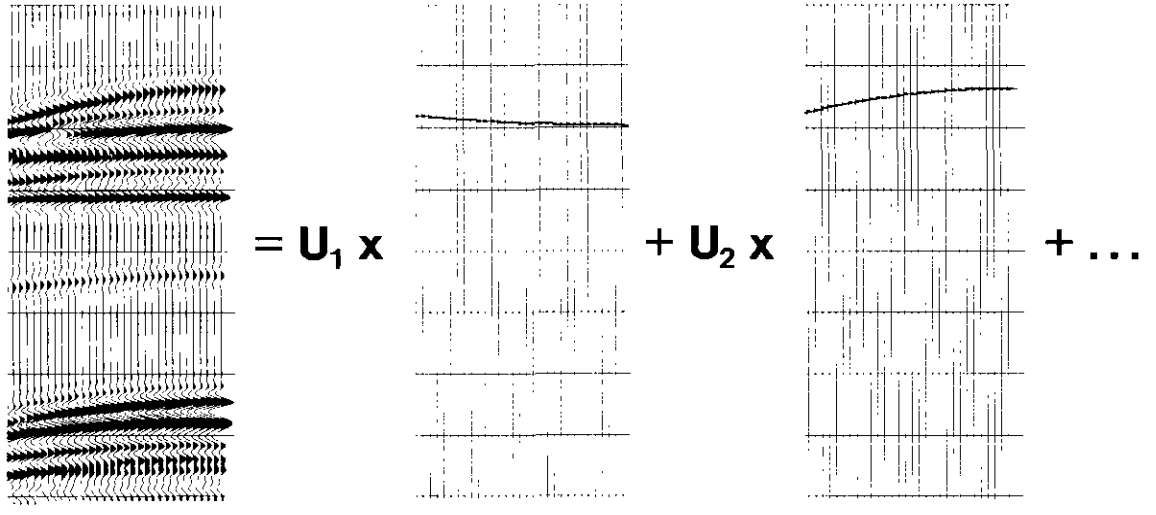


**Fig. 2.** In the modelling interpretation, each input NMO-corrected profile is represented as a linear combination of weighted parabolic events.

stant amplitude curves could possibly represent real seismic data with its variations in amplitude and waveform. The question is entirely equivalent to how a series of uniform sine waves can model a complex time series in the Fourier Transform. The answer is that we use a very large number of closely spaced parabolae which constructively interfere to produce the resulting image. Figure 3 demonstrates the case of four parabolic curves for each of three zero-offset time samples. In practice, 20 to 30 curves are used over some specified range of move-outs. With an 800-ms data window at 2-ms sample rate, this would mean that $400 \times 20 = 8000$ parabolae are being used to model the profile of Figure 2.

Figure 4 shows the result of solving the least-squares system (16) for this model. Each parabola is parameterized by its zero-offset time and its 'move-out', or time difference between far-offset and zero-offset time:

$$\text{MOVEOUT} = \text{FAR-OFFSET TIME} - \text{ZERO-OFFSET TIME} \qquad (21)$$

In this case, the variable, p , was discretized at 20 values corresponding to move-outs ranging from −10 ms to +200 ms. The right hand side of Figure 4 plots the coefficients $U(p, \tau)$. In fact, equation (16) was solved at a series of discrete frequencies from 10Hz to 100Hz and $U(p,\tau)$ was calculated by using equation (11).

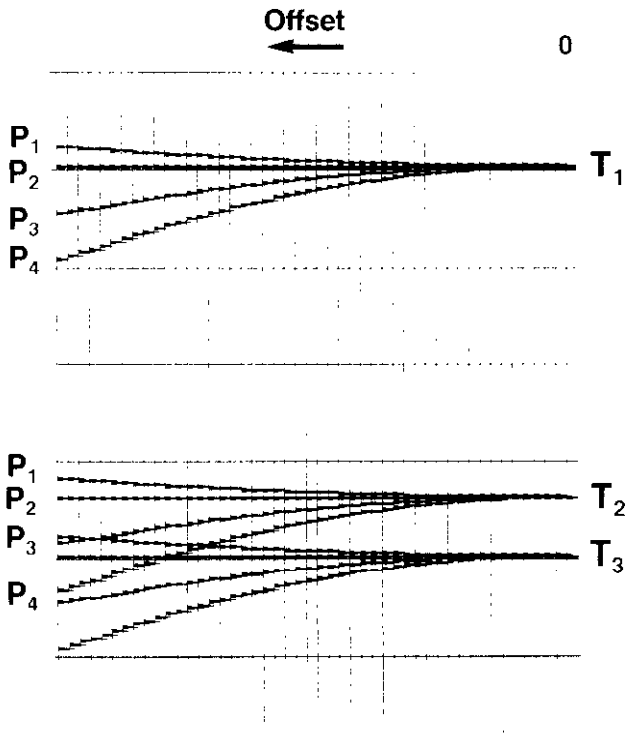


**Fig. 3.** For each zero-offset time, T, a range of parabolae is used, effectively spanning the profile with a large number of parabolae.

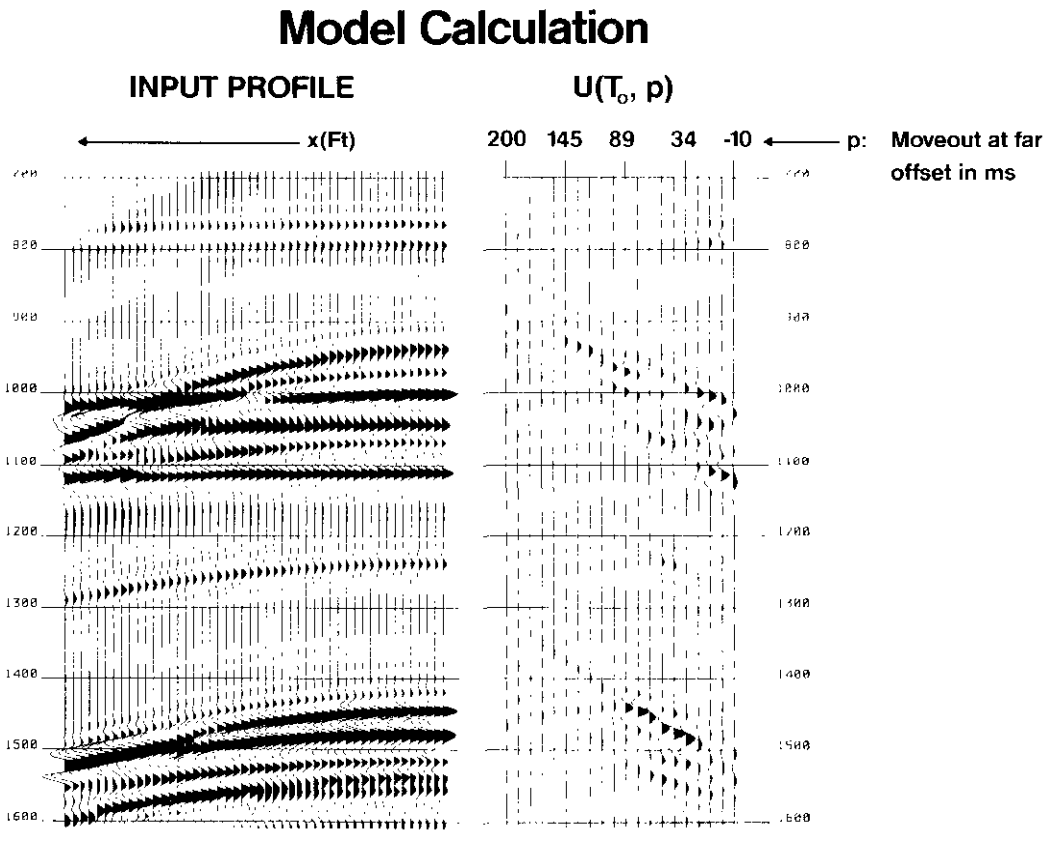


**Fig. 4.** Plot of parabolic coefficients $U(p,\tau)$ calculated for input model by using equation (16).

The transform $U(p,\tau)$ can now be interpreted in much the same way as the constant-velocity stack of Figure 1, except that 'move-out' replaces velocity on the horizontal axis. Since the input model is NMO-corrected, we can expect primary energy to map to events at around 0-ms move-out, while undercorrected multiples should map to higher move-outs. This has in fact taken place, and primary energy can be discerned at 780 ms, 1000 ms, and 1110 ms. Strong multiples appear at 920 ms, 980 ms, 1080 ms, and below 1200 ms. The input model was calculated and NMO corrected by using exact hyperbolic move-outs, so the sharpness of the imaged energy on the $U(p,\tau)$ plot is evidence of the validity of the parabolic approximation.

Having calculated the coefficients $U(p,\tau)$, the forward model can now be generated by using equation (10) with $n(h,t)$ set to zero. This result is shown in Figure 5. The left panel of the figure shows the original synthetic data set, the centre panel shows the model result, and the right panel shows the residual error calculated by subtracting the model from the input. As expected, the model is a close approximation to the input. In fact, it is easy to show that the residual error could be reduced to zero by using a sufficiently large range of move-out values p.

For the purpose of multiple elimination, it is now necessary to produce a model containing the multiple energy only. This is done by 'filtering' the coefficients of Figure 4; that is, setting a subset of the coefficients to zero. The procedure is directly comparable to filtering in the F-K domain, and one would expect that rules of thumb appropriate to that domain should be applicable here. In particular, sharp cutoffs have been observed to generate artifacts analogous to the Gibb's phenomena well known in F-K filtering. Although it has not been tested, it should be possible to reduce this problem by tapering between the pass and reject zones in the transform domain. For these examples a sharp cutoff was actually used without any apparent ill effects. Setting to zero all coefficients with move-outs less than 30 ms produced the model result in Figure 6. Comparing it with Figure 5, we can see that the primary events at 780 ms, 1000 ms and 1110 ms are largely missing and the multiple events are isolated. Subtracting the multiple model from the input data produces the final multiple-attenuated result in the right panel of Figure 6.

The model result in Figure 6 confirms that the algorithm is very powerful at attenuating long-period multiples. A very satisfactory feature is that, where multiples have been attenuated, the attenuation is equally good at all offsets. This is in contrast to the use of F-K filtering for multiple elimination, where it is commonly observed that the small-offset or 'near' traces are handled less than satisfactorily. There is of course no mystery in the fact that these two algorithms perform differently on this data set. The inverse velocity stacking algorithm is based on a parabolic model and is ideally suited to modelling parabolic or approximately parabolic events. The F-K algorithm is based on a plane-wave model and is ideally suited to modelling linear events. The trajectories of long-period multiples after NMO-correction at the primary velocity are more closely approximated by parabolae than by straight lines.

Another important feature of the algorithm is evident in Figure 6: while the primaries should be NMO-corrected, it is not necessary that the correction be exactly right.

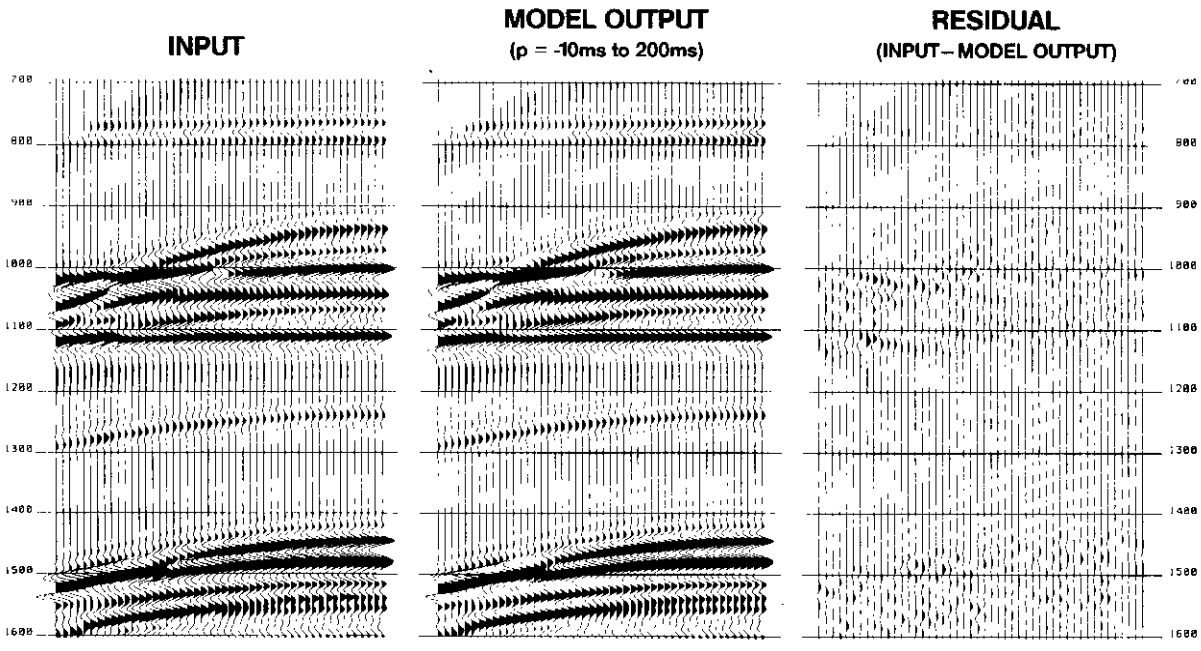


**Fig. 5.** Input synthetic, model calculated by applying forward equation (10) with coefficients displayed in previous figure, and residual noise resulting from subtracting model from input data.

The event at 1000 ms is obviously undercorrected. The performance of the algorithm is in no way degraded by this error as long as the degree of undercorrection is not such as to cause the primary to appear in the multiple zone; *i.e.*, greater than 30-ms move-out. It is now possible to perform a residual velocity analysis on the output of Figure 6 and refine the velocity estimate without the strong interfering multiples.

A final point should be made about the algorithm, which is not particularly obvious in Figure 6. Since the L-matrix defined by equation (15) contains precise information concerning the number and distribution of offsets, no artifacts will be generated either by the boundaries of the model or by uneven trace spacing. This is another feature in contrast with F-K algorithms, which assume periodic boundary conditions and uniform spacing. It makes the parabolic algorithm particularly attractive for use on crooked-spread or 3-D data sets.

## Real Data Results

The inverse velocity stack algorithm will be applied to two real data sets. A shot profile from the first data set is shown on the left of Figure 7. This profile is NMO-corrected and the zone of interest centres around the reflector at about 1100 ms. A strong multiple with about 100 ms residual move-out appears at a zero-offset time of 1020 ms and cuts through the primary event at an offset of approximately two-thirds of the spread length. The shot profile has had deconvolution and near-surface static corrections applied, and is fully processed with the exception of the final filter.

The right side of Figure 7 shows the total model generated by solving equation (16) for this data set. The discrete set of parabolae used was identical to that in the preceding model result. A limited window of input data, from 650 ms to 1500 ms, was analyzed to reduce computer run-time. Figure 7 shows the result of modelling both primary and multiple energy. As explained above, each side of the spread is modelled independently, which produces a slight discontinuity at the centre of the model profile. To evaluate how well this model fits the input data, Figure 8 shows the result of subtracting one from the other. Obviously, any segments of reflectors or coherent energy that the eye perceives as signal on the input profile have been modelled, as evidenced by the total lack of coherent signal within the analysis window of the residual profile of Figure 8. What now stands out is the low-frequency ground roll, which has been effectively ignored by the algorithm because of its dissimilarity to the modelling parabolae.

For this particular data set, the multiple cut-off has been set at 80 ms move-out, and the multiple attenuated result is shown in Figure 9. The major multiple event at 1020 ms has been largely attenuated, as have some shallower multiples at around 900 ms. The primary event at 1100 ms has been preserved and in fact enhanced by suppressing the interfering multiple energy on the far offsets. It appears that residual multiple energy between 1100 and 1200 ms has been left, presumably because its moveout is less than 80 ms.

The common offset stacks of Figure 10 are useful in giving an overview of the performance of the algorithm over a larger data volume. Each common offset stack was calculated by analyzing traces from 24 adjacent

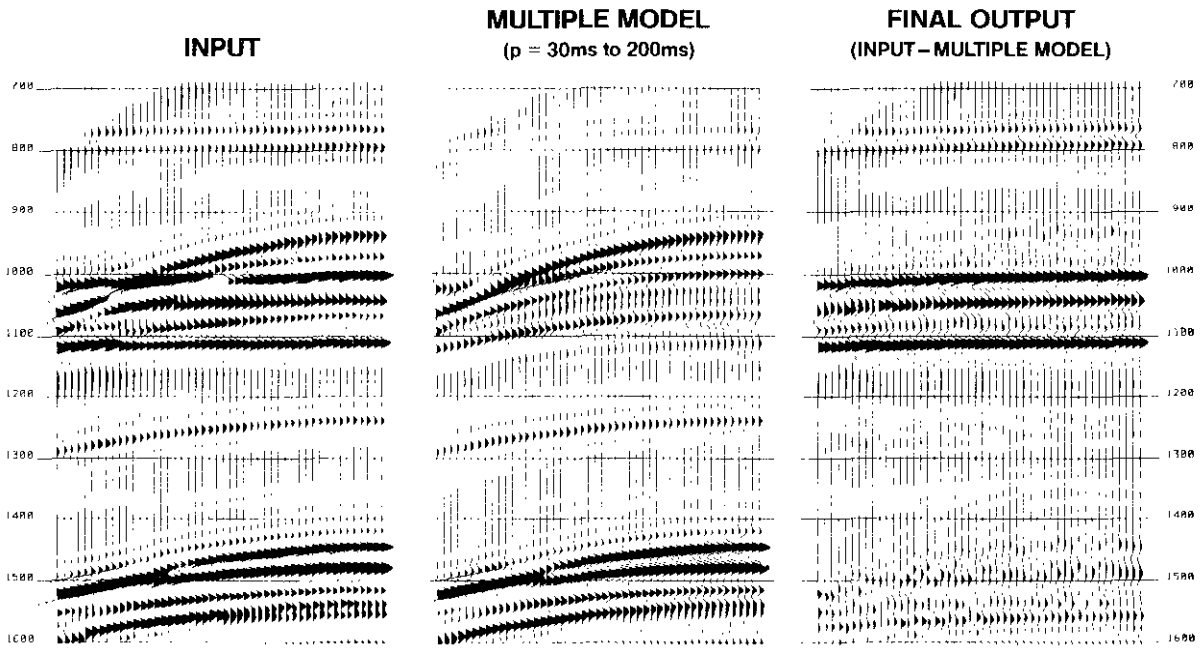


**Fig. 6.** Input synthetic, multiple model calculated by applying forward equation (10) with coefficients for parabolae with move-outs from 30 ms to 200 ms, and multiple attenuated result

common-depth-point gathers and stacking traces with identical or similar source-receiver offsets. The result is an 'average' common-depth-point gather where the stacking has enhanced the signal-to-noise ratio while preserving offset-dependent characteristics. The three panels of Figure 10 respectively show the common offset stacks over the same data traces before multiple elimination, after applying the inverse velocity stack algorithm to the shot profiles as described above, and after applying the F-K multiple elimination procedure of Ryu (1980) to the shot profiles. The latter procedure consists of NMO-correcting the data at a velocity intermediate between that of the primary and multiple velocities, and using an F-K filter to remove down-dipping energy. Both procedures have been very effective in suppressing the strong multiple events between 1000 and 1200 ms. In fact, the

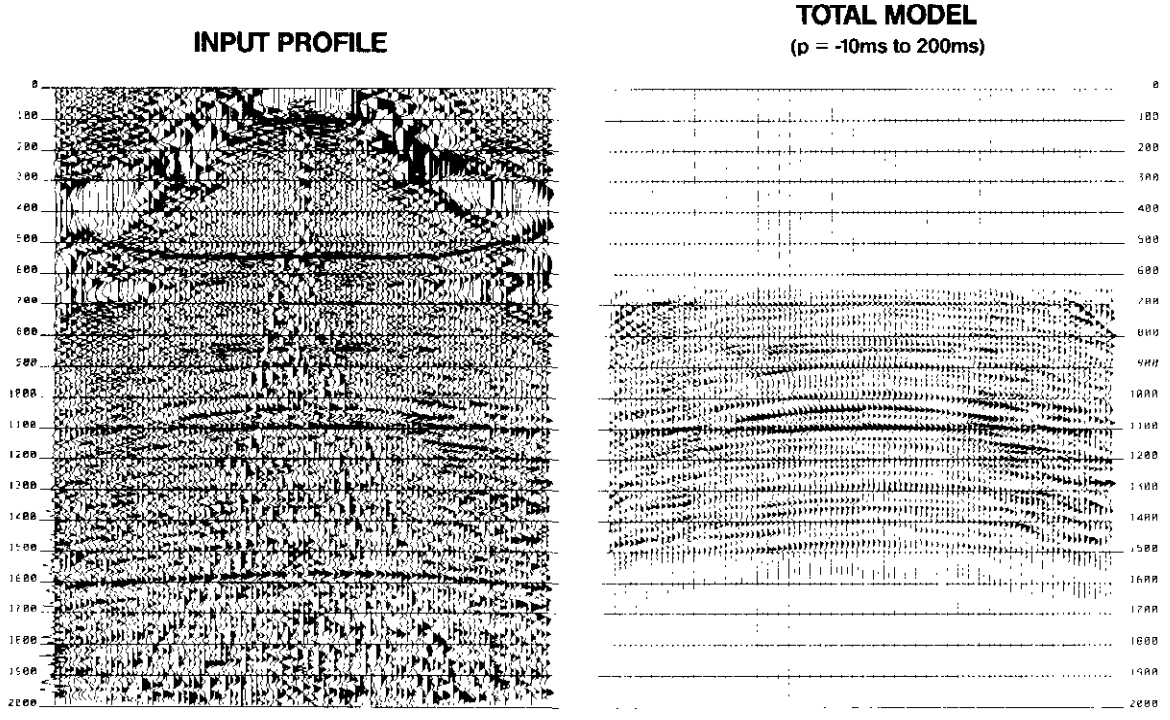


Fig. 7. Input real-data shot profile with total model calculated within data window from 650 ms to 1500 ms.

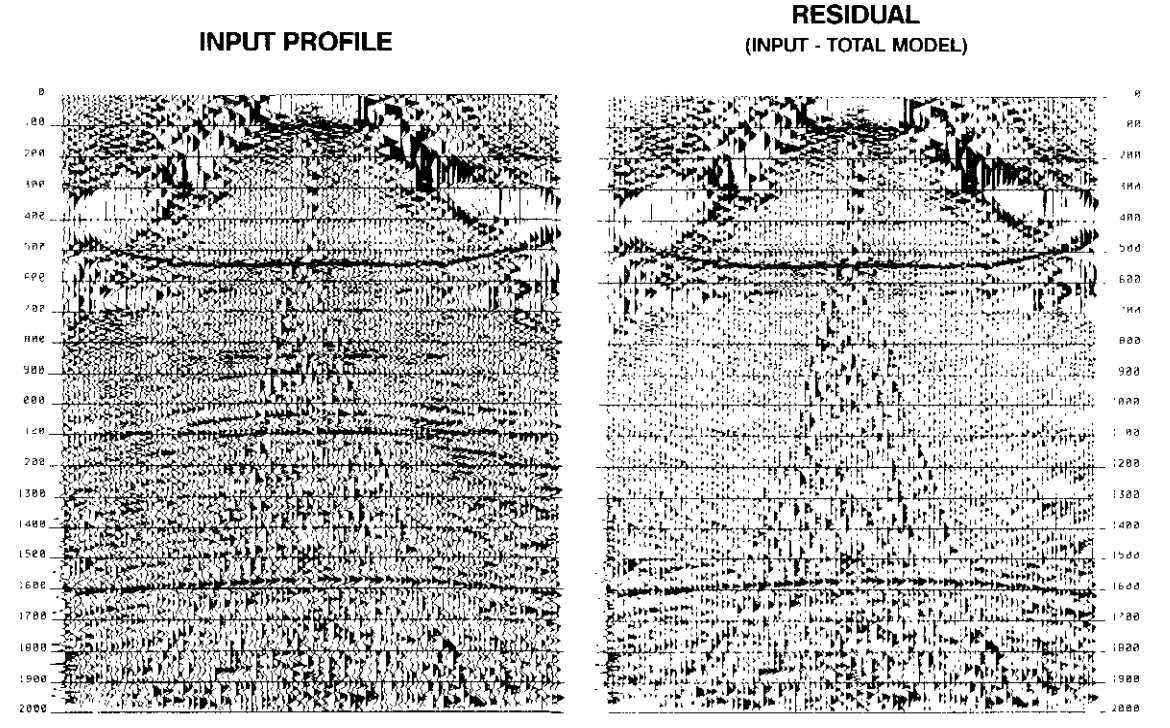


Fig. 8. Input real-data shot profile with result of subtracting total model from input data

two results are surprisingly similar at the far offsets where primary and multiple energy interfere destructively. The major differences occur on the near-offset traces where the F-K algorithm has left significant multiple energy, while the inverse velocity stack algorithm has been effective at all offsets.

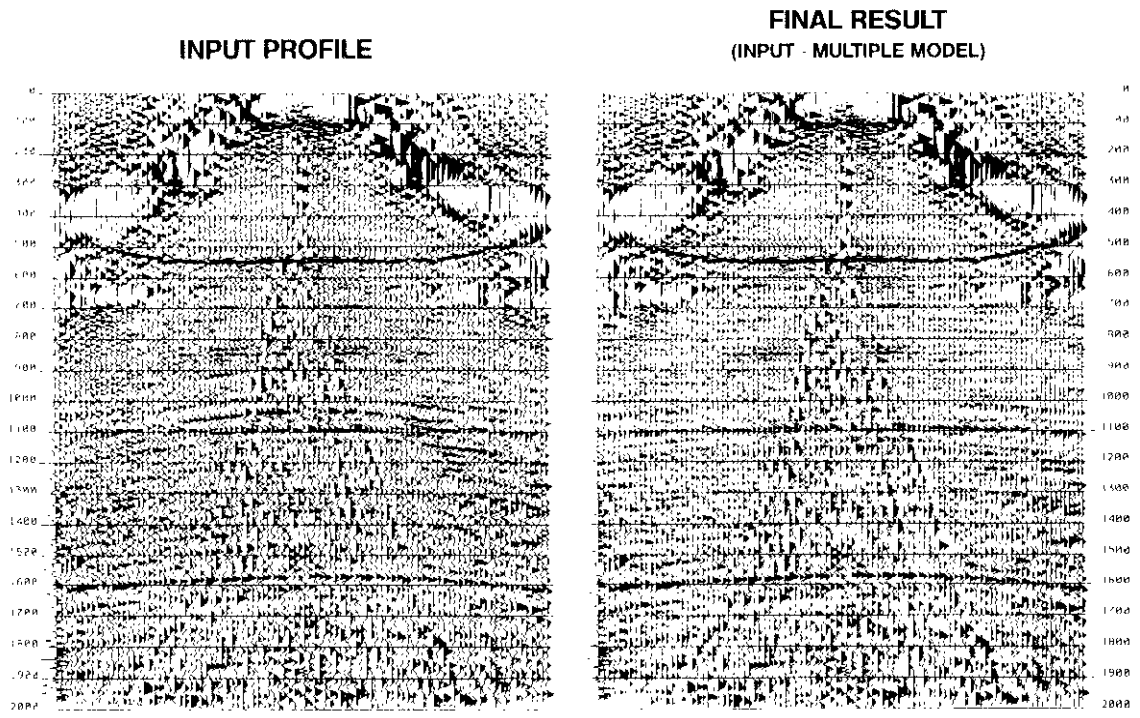


**Fig. 9.** Input real data shot profile with multiple-attenuated result.

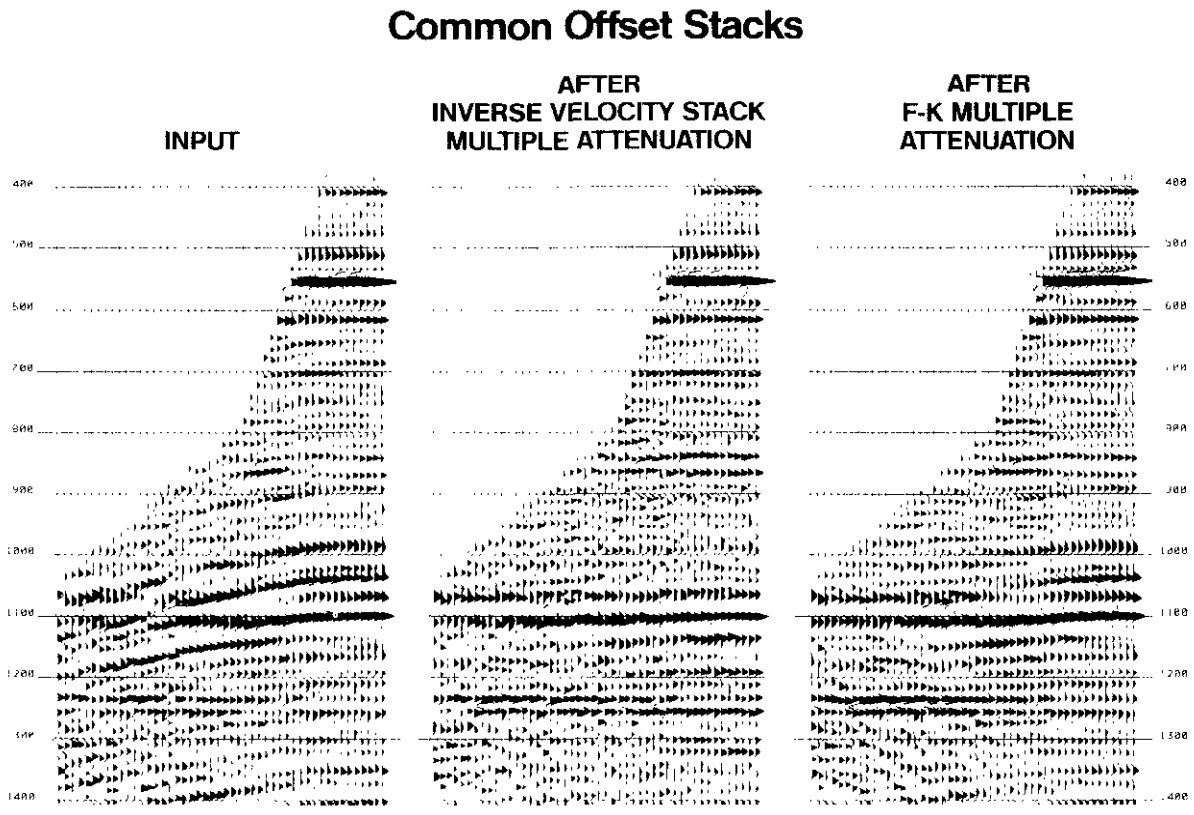


**Fig. 10.** Common offset stacks calculated from data before multiple attenuation, after inverse velocity stack multiple attenuation, and after F-K multiple attenuation

The second real-data result is shown in Figures 11 to 14. The first two, Figures 11 and 12, show common offset stacks before and after multiple elimination. The zone of interest, from approximately 700 to 1000 ms, is strongly contaminated with undercorrected multiple energy as in the previous example. Again the inverse velocity stack algorithm was applied to a limited time window: from 600 to 1200 ms in this case. The range of parabolic move-outs was set from −10 ms to +200 ms, with the cut-off move-out separating multiple from primary energy set at +30 ms. Comparing Figures 11 and 12, we see a very significant change in the reflector quality as a result of multiple attenuation. It should be noted that each common offset stack was scaled with a short window AGC. This accounts for the increase in amplitude observed on primary events, particularly between 700 and 900 ms.

Figures 13 and 14 compare the final stacked sections before and after multiple elimination. The processing flow was identical in each case except for the inverse velocity stack step, which was applied to the shot profiles just before final stack. The NMO and statics corrections were identical, as were the trace scalings before stack. The final stacked traces were scaled by deriving a single multiplier for each trace to equalize the RMS amplitude over the zone of interest. In general, we see a very significant improvement in continuity over many areas of the zone of interest, which is consistent with the changes observed on the common offset stacks of Figures 11 and 12. Experience has shown that this level of improvement on the stacked section is not achieved in every case — stacking is itself a powerful multiple attenuation mechanism. However, it is clear that where multiples dominate the recorded seismograms to the extent visible in Figure 11, an algorithm such as inverse velocity stacking can substantially improve the imaging of weak primary reflectors.

Both the model and real data examples have shown the performance of the algorithm on shot-ordered profiles. Theoretically, this approach should be applicable only to plane-layered, zero-dip data. Practical experience has shown that, in fact, the algorithm is quite robust in the presence of moderate structural deviations from the ideal, as can be seen in the previous examples. One reason for this is that, by modelling the multiple and subtracting it from the input profile, structural anomalies such as faults will tend to be poorly modelled and hence left in the data as noise. In some circumstances, however, structural anomalies like diffraction patterns may be modelled as multiples and suppressed by the algorithm. In these cases, this algorithm should be applied in the CDP domain, where all primary energy should ideally appear as zero-dip events after normal move-out.

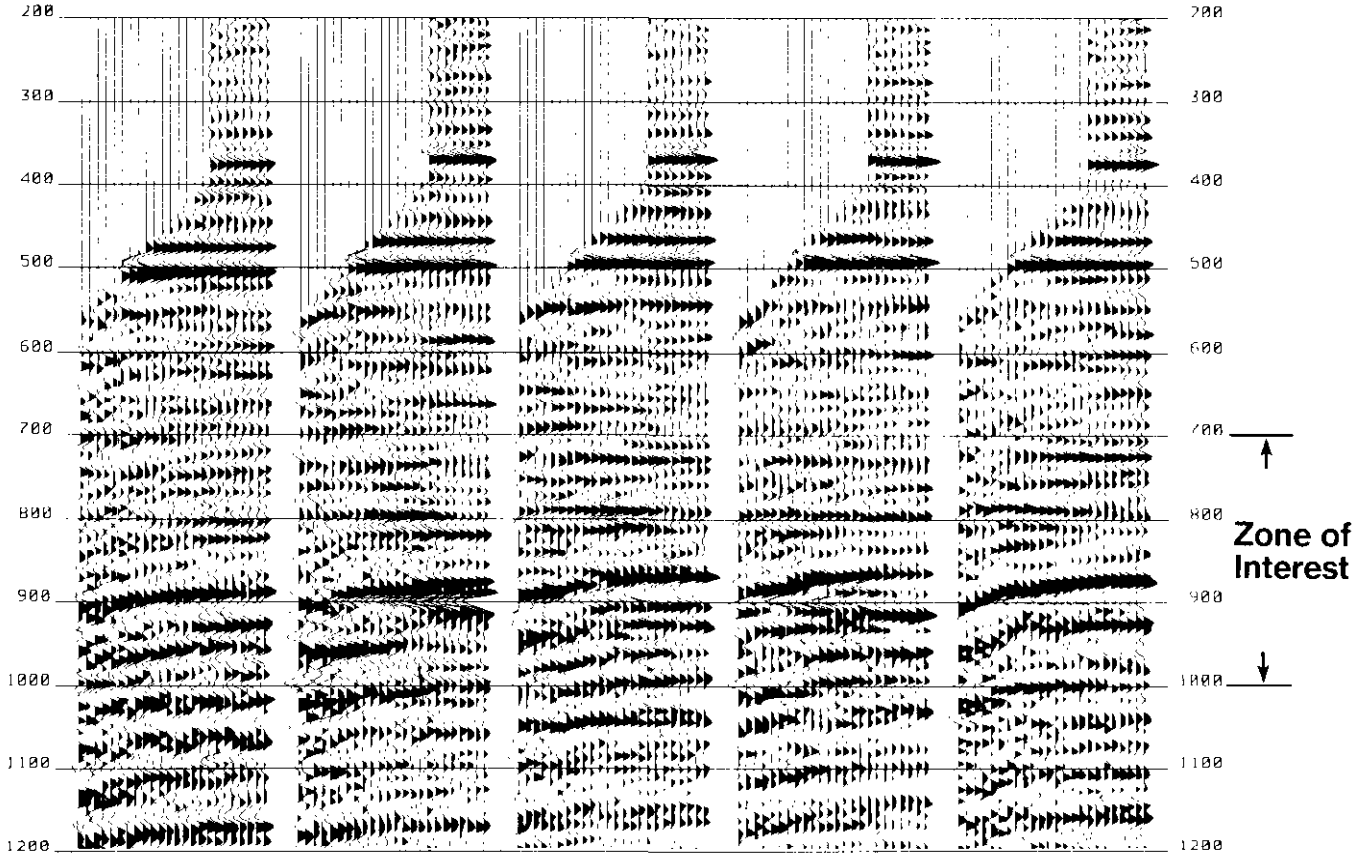


**Fig. 11.** Second real-data set common offset stack before multiple attenuation.

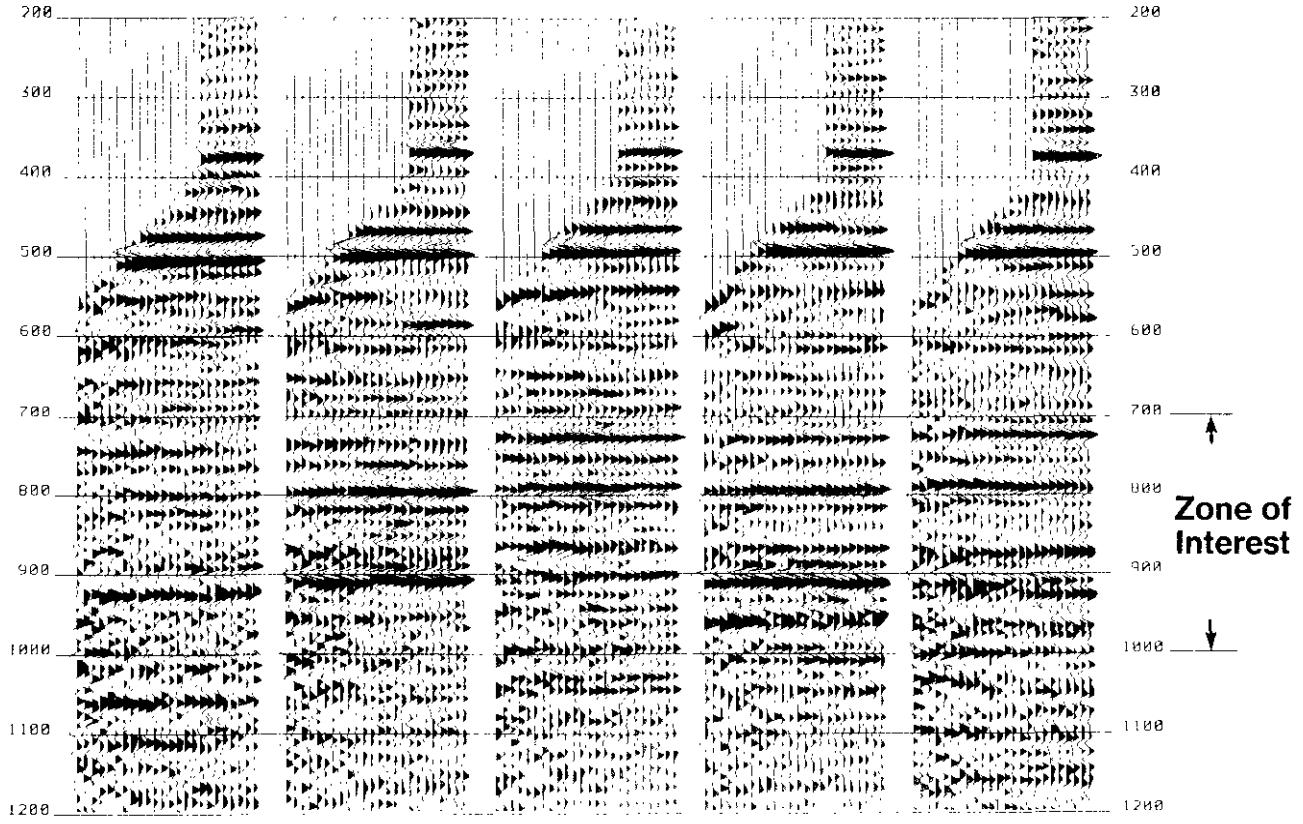


**Fig. 12.** Second real-data set common offset stack after inverse velocity stack multiple attenuation

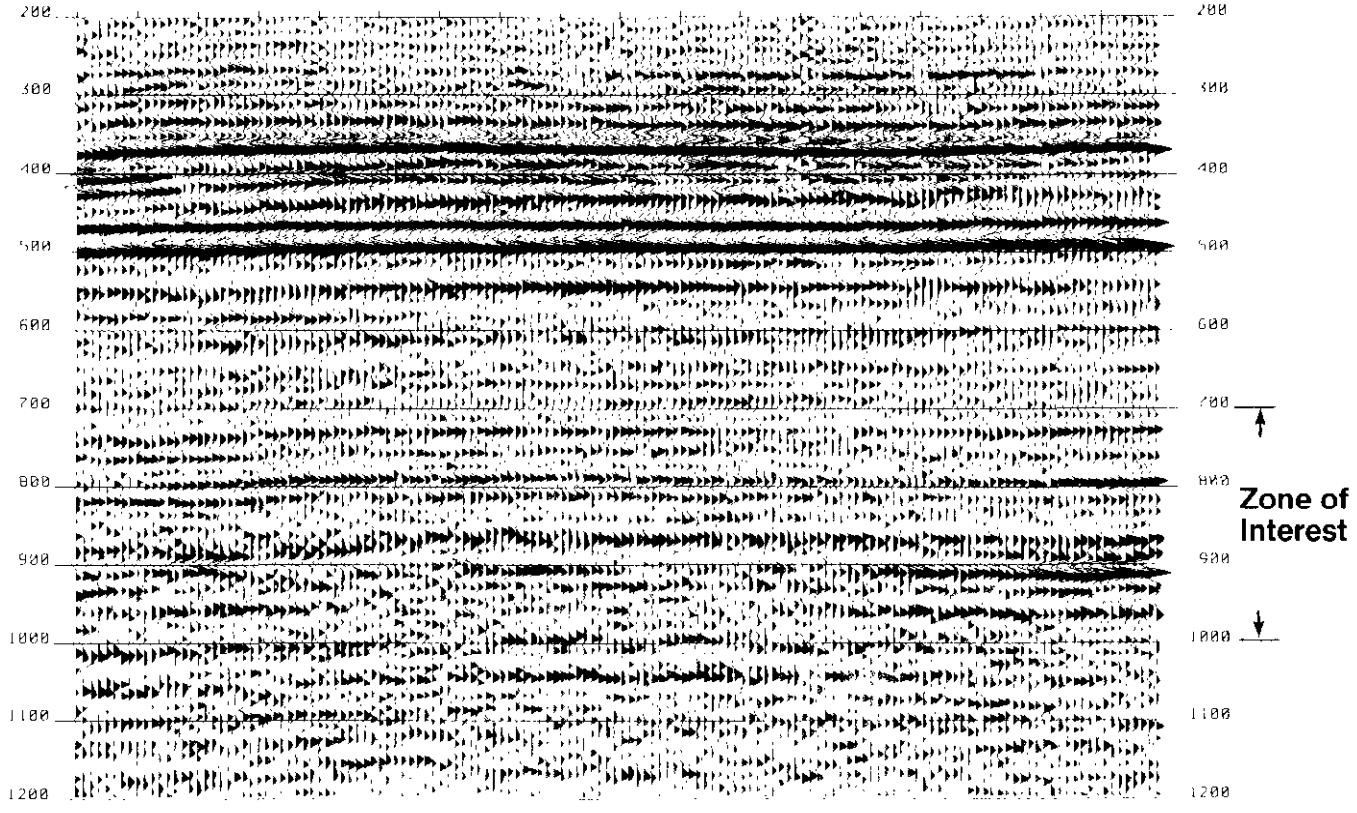


**Fig. 13.** Second real-data set conventional stack without multiple attenuation

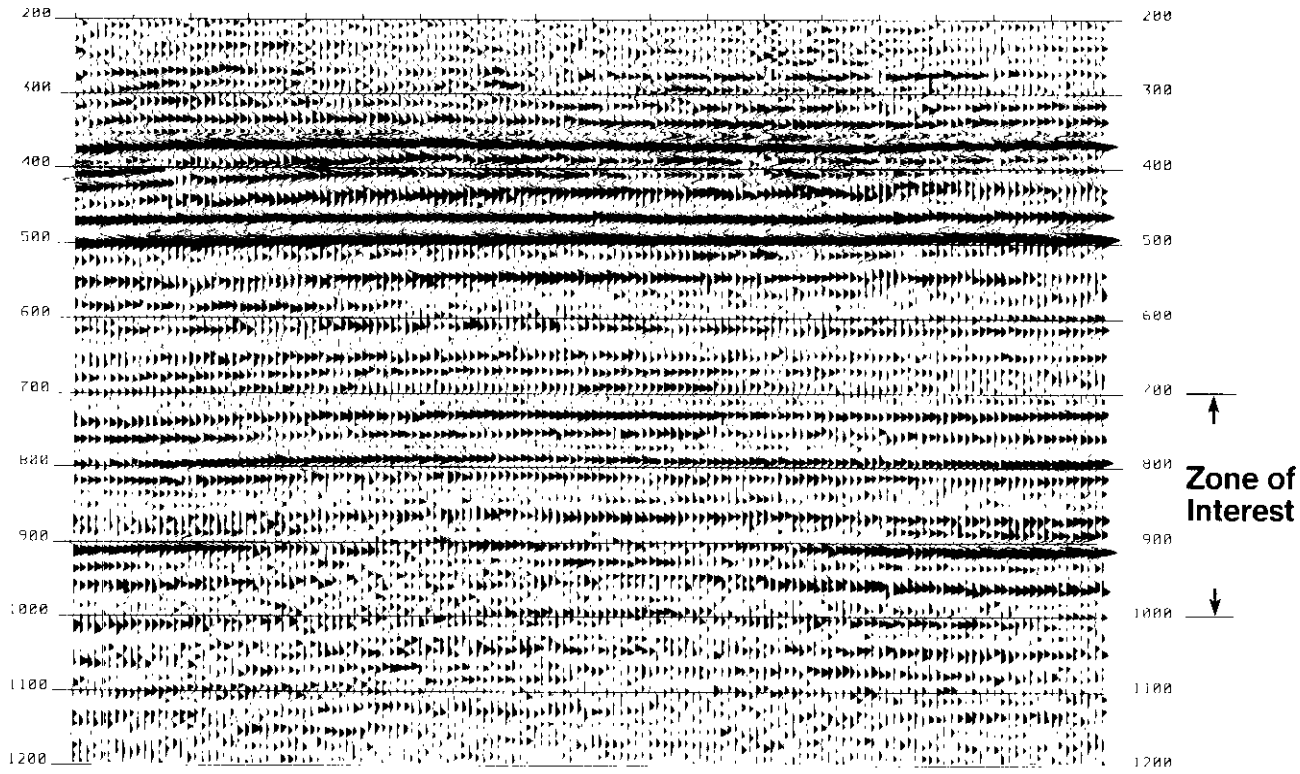


**Fig. 14.** Second real-data set stack after inverse velocity stack multiple attenuation.

## Conclusions

This paper has shown how the Inverse Velocity Stack algorithm of Thorson can be modified to incorporate a parabolic approximation, and thus provide a useful tool for multiple elimination. Some of the features that make it particularly attractive are:

1) It achieves multiple attenuation at all offsets equally.

2) It requires no knowledge of the multiple-generating mechanism.

3) It requires no detailed knowledge of the multiple and primary velocities.

4) It will attenuate a wide range of multiples with variable moveouts.

5) It will accommodate variable or nonuniform acquisition geometry, while minimizing 'edge effects' associated with limited data aperture. This makes the algorithm attractive for application to 3-D data sets.

Limitations associated with the method are:

1) Computation time is significantly greater than for standard techniques.

2) Multiples must have sufficient move-out discrimination to be attenuated. This issue was not addressed in this paper, but experience has shown that, while very fine discrimination may be achieved on model data, real data, with their variable amplitudes and waveforms and their additive noise, demand at least 30-ms move-out from near trace to far trace to be effective.

3) As with F-K filtering, sharp cut-offs in the transform domain may produce artifacts as a result of Gibb's phenomenon.

## References

Hampson, D. and Dunham, A., 1985, Long period multiple elimination through inverse velocity stacking: Presented at the Annual Convention of the Canadian Society of Exploration Geophysicists, Calgary, Alberta.

Ryu, J.V., 1980, Decomposition of seismic gathers into velocity components by a space-time filter: Presented at the 50th Annual Meeting of the Society of Exploration Geophysicists, Houston, Texas.

Thorson, J.R., 1984, Velocity-stack and Slant-stack Inversion Methods: Ph.D. thesis, Stanford University.

_____ and Claerbout, J.F., 1985, Velocity-stack and slant-stack stochastic inversion: Geophysics, v. 50, p. 2727-2741.